Electron Transport and Thermoelectric Performance of Defected Monolayer MoS_2

Munish Sharma[1, 2, a)], Ashok Kumar[3] and P.K.Ahluwalia[1]

[1)] *Department of Physics, Himachal Pradesh University, Shimla 171005, India*

[2)] *Department of Physics, School of Basic and Applied Sciences, Maharaja Agrasen University, Baddi 174103, India*

[3)] *Department of Physical Sciences, School of Basic and Applied Sciences, Central University of Punjab, Bathinda 151001, India*

(October 24, 2018)

[a)]Corresponding Authors

Email: munishsharmahpu@live.com

Abstract

Electronic and thermoelectric properties of a two-dimensional MoS_2 monolayer containing atomic defects are investigated using density functional theory. All the atomic defects have been found to exhibit endothermic nature. Electronic structure of MoS_2 shows tuneability of band gap with the atomic defects. The MoS_2 vacancy in pristine monolayer makes it magnetic and narrow band gap semiconductor. The spin-polarized character of the monolayer with defects is clearly captured by the tunneling current calculated in the STM-like setup. A relatively low thermal conductivity has been observed in monolayers with defects as compared to pristine form resulting in enhanced room temperature figure of merit as high as 6.24 and 1.30 respectively. The results presented open up a new window for the use of monolayer MoS_2 in electronic devices, thermal management and thermoelectric devices.

1. Introduction

The discovery of graphene [1] opened a flood gate to the world of two dimensional materials. The award of noble prize to A. K. Geim and K. Novoselov in 2010 clearly acknowledge the novelty of graphene as a material of immense possibilities [2-5]. However, absence of inherent band gap in graphene hindered its direct applications.

The quest for finding new materials resulted in a large group of graphene like materials which include: hexagonal boron nitride (h-BN), silicene, germanene, silicon carbide (SiC), gallium nitride (GaN), zinc oxide (ZnO) and transition metal dichalcogenides (TMDs) [6] etc. The two dimensional (2D) alternatives to graphene such as MoS_2 and other few-layer transition metal dichalcogenides (TMDs, MX_2 where M: Mo, W; X: S, Se) are offering opportunities for energy conversion [7], sensing [8-11], super lubricity in nano-machines [12], photoelectronic application [13] and electronic device applications [14-16]. Despite having graphene like quasi-two dimensional structure (tri-atomic) MX_2 in addition has broken inversion symmetry and spin orbital coupling (SOC) originating from d-orbital of metal atoms. The effect of SOC on electronic properties has been observed for MX_2 systems with small effect for Mo based monolayer systems as compared to other TMD's [17-19]. Note that the characteristic features in structural and electronic properties MX_2 monolayers remain same.

Among the MX_2 family, MoS_2 has always remained a prototype material from this family of TMD's for various applications. Monolayer MoS_2 could be synthesized by mechanical exfoliation technique [20], liquid exfoliation [21] and chemical synthesis techniques such as chemical vapor deposition (CVD) [22, 23], physical vapor deposition (PVD) [24] etc. Note that a defect-free structure is not a practical reality, as atomic defects are often observed in experiments [25]. Recent investigations suggest that the carriers mobility decreases in samples prepared by chemical methods as compared to samples prepared by mechanical exfoliation technique [22, 26]. It was reported that this decline in mobility generally takes place because of structural flaws/defects [25-27].

Several studies have focused on the thermoelectric properties of single layer and few layer MoS_2 [13, 28-36] to solve energy issues. The efficiency of a thermoelectric material could be

quantified by figure of merit, $ZT = \frac{S^2 \sigma T}{k_{ph} + k_e}$, where, S is the Seebeck coefficient, σ is electrical conductivity, T is temperature and k_e and k_{ph} electronic thermal conductivity and lattice thermal conductivity respectively. Since all these parameters are interdependent, enhancing the figure of merit (ZT) is a challenging task. The room temperature figure of merit (ZT) lies between 0.02 to 0.53 [37] for monolayer MoS_2. Recent experiments have demonstrated that single layer MoS_2 show its potential as a good thermoelectric material with a large value of the Seebeck coefficient [13, 32]. According to the formula for figure of merit, ZT, reducing the thermal conductivity is a promising route to improve ZT in low dimensional materials [38, 39]. Numerous studies have shown that vacancy, defects, and doping have magnificent effect on thermal conductivity [39-43] in graphene and MoS_2; thus influencing the ZT.

Inspired by experimental and theoretical studies we focus in this paper on understanding the role of defects in modulating the electronic and other properties of MoS_2 which are of significant impact on their increasing use in device applications, we look at the influence of four different types of atomic defects viz. V_S (one S vacancy), V_{Mo} (one Mo vacancy), V_{MoS} (one Mo and one S vacancy), V_{MoS_2} (one Mo and two S vacancies) on structural, electronic, magnetic and thermoelectric properties of MoS_2.

2. Computational Details

The pristine MoS_2 monolayer has been modeled by 4x4 supercell having 48 atoms. A sufficient vacuum of ~20 Å along the z-direction was used to minimize interactions between 2D periodic images. First principle spin polarized calculations, implemented in the Vienna *ab initio* simulation package (VASP) [44, 45], have been carried out within the framework of density functional theory (DFT). The projector augmented-wave (PAW) method [46] was employed to represent the electron-ion interactions. The generalized gradient approximation (GGA) using Perdew-Burke-Ernzerhof (PBE) functional has been used to treat the exchange and correlation interactions [47]. The plane wave cutoff energy has been set to 400 eV. The Monkhorst-Pack scheme with a *k* mesh of 10x10x1 has been used to sample the irreducible part of Brillouin zone.

The structural relaxations have been carried out using conjugate gradient technique. All the structures have been fully relaxed until the residual force on each atom is converged to less than 0.02 eV/Å. The electronic density of states (DOS) was calculated with Gaussian broadening parameter of 0.02 eV. The energy convergence criterion has been set to 10^{-6} eV self-consistency for electronic steps. The transport coefficients; Seebeck coefficient (S), electrical conductivity (σ) and electronic thermal conductivity (k_e) were obtained by semi-classical Boltzmann theory as implemented in Boltztrap code [48].

3. Results and Discussions

Our investigations begin with the structural optimization of 4x4 supercell of pristine MoS_2 with cell dimensions 12.72 Å x 12.72 Å. Figure 1 depicts fully relaxed structure of pristine MoS_2 and MoS_2 containing atomic defects. The introduction of such atomic defects are very likely in experiments during synthesis and is expected to influence electronic, magnetic and thermoelectric properties of 2D MoS_2 as compared to its pristine form.

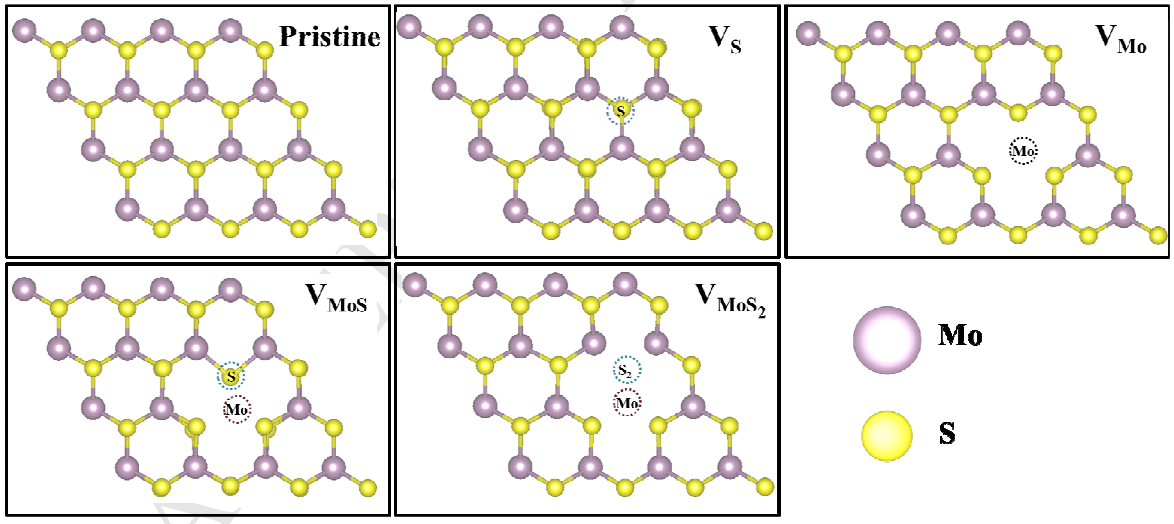

Figure 1. Optimized structures of monolayer MoS_2 with no vacancy (Pristine), with Mo vacancy (V_{Mo}), with MoS vacancy (V_{MoS}) and MoS_2 vacancy (V_{MoS2}).

The formation energy of atomic defects (E_f) has been calculated using following formula.

$$E_f = (E_{defect-monolayer} + E_{atomic-defect}) - E_{pristine-MoS_2}$$

Here, $E_{defective\text{-}monolayer}$ and $E_{atomic\text{-}defect}$ represent the total energy of monolayer MoS_2 with atomic defects and total energy of removed atomic defect respectively. The calculated defect formation energy is found to be 5.81 eV for V_S type vacancy which is much lower than the formation energy of all other types of atomic defects under investigations (supplementary table S1). Our calculated formation energy for the case of V_S and V_{Mo} is in close agreement with the earlier reported values of 5.72 eV and 13.5 eV respectively [49, 50]. The lower formation energy for the case of V_S type vacancy indicates the ease of formation of such defects among all other types. Note that the positive E_f indicates an endothermic nature of such defects.

In order to find the stability of MoS_2 with the presence of defects total energy per atom of pristine and MoS_2 with defects is calculated (E_{total}/n ; where n is total number of atoms in supercell). Total energy per atom for pristine and MoS_2 with S vacancy is ~0.2 eV lower (more negative) than other types of defects (supplementary Table S1) indicating pristine MoS_2 and MoS_2 with S defect more stable as compared to other cases.

Next, we pay our attention to the structural distortions taking place due to presence of atomic defects in MoS_2. A careful analysis of the relaxed atomic structure reveals that structural distortions takes place around the defect only. We find that Mo-Mo distance ($d_{Mo\text{-}Mo}$) decreases by 2.66 % and 11.45 % for the V_{Mo} and V_{MoS_2} vacancy, while for V_S and V_{MoS} type of vacancy atomic distortions are of the order of 0.05 Å as compared to pristine MoS_2. These atomic distortions are expected to result in different atomic hybridizations which can modulate the electronic structure and magnetic properties of pristine MoS_2.

3.1 Electronic and Magnetic Properties

Figure 2 shows the electronic band structure of pristine and defective MoS_2. In the previous investigations electronic band structure of pristine MoS_2 shows direct band gap character which is confirmed by PL spectra in experiments [15, 51]. Our result is consistent with the earlier reports [15, 51, 52].

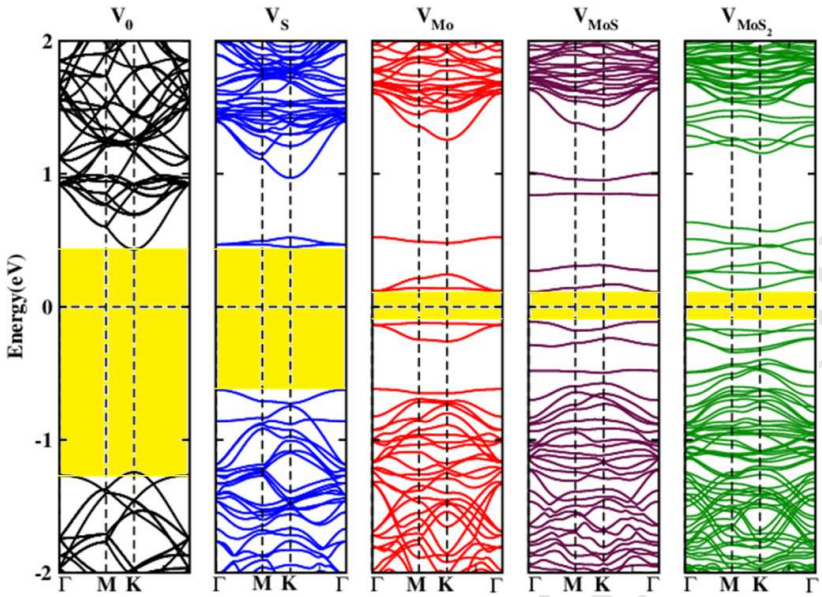

Figure 2. Spin Polarized band structures of pristine MoS_2 and MoS_2 containing different atomic defects. Shaded region indicated the band gap. Fermi level is set at 0 eV.

The electronic band structure shows tuneability with the introduction of defects. The direct band gap of 1.60 eV gets decreased in defective monolayers. The band gap is found to be 1.07 eV for V_S type defect while band gap reduces to ~ 0.22 eV for all other types of defects. A direct to indirect band gap transition has been observed for defective MoS_2 due to appearance of defect energy levels in the vicinity of Fermi level. To gain an insight into localization of Valance Band Maxima (VBM) and Conduction Band Minima (CBM) we have calculated the spin resolved atom projected band structure which is presented in figure 3. It can be seen from figure 3 that the maximum contribution to the VBM and CBM originates from the Mo atom. A similar feature could be seen for the V_S type of defect. For the case of V_{Mo} and V_{MoS} , the defect energy states in the valance band arises from S atom while CBM show contribution from both Mo and S atom. Note that for V_{MoS_2} type defect spin up VBM and CBM are localized on both Mo and S atom while for spin down polarization VBM and CBM are localized on Mo and S atom respectively.

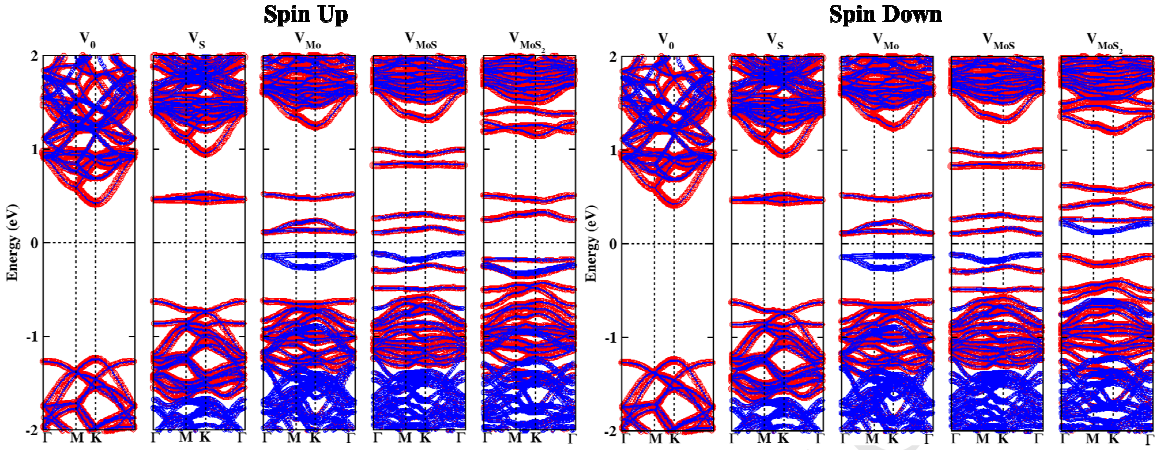

Figure 3. Spin resolved atom projected band structure for pristine MoS_2 and MoS_2 with atomic defects. Red (Blue) color bands are energy bands due to Mo (S) atom respectively. The width of the band represents the spectral weight.

The change in electronic band structures due to atomic defects could be understood by examining the charge density difference profile (defined by, $\Delta\rho = (\rho_{defective-monolayer} + \rho_{atomic-defect}) - \rho_{pristine-MoS_2}$). It can be seen from figure 4 that charge redistribution is more pronounced in the defect region. For the case of V_{MoS_2} the charge accumulates between Mo atoms indicating some sort of strong interaction between Mo atoms. This could be attributed to the structural distortion taking place due to defects.

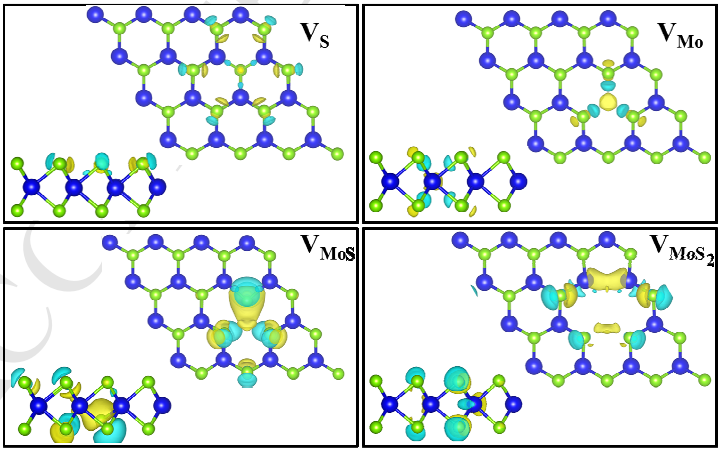

Figure 4. Top and side view of charge density difference profiles for S vacancy (V_S), Mo vacancy (V_{Mo}), MoS Vacancy (V_{MoS}) and MoS_2 Vacancy (V_{MoS_2}). Blue and green balls represent Mo and S atoms respectively. Yellow/Cyan color depicts charge accumulation/depletion. Isosurface value is set to 0.02 e/Å^3.

In order to get further insight into the presence of defect states we have analyzed spin polarized density of states (figure 5). The finite density of states in the vicinity of Fermi level for MoS_2 with defects clearly depicts the presence of defect states. The presence of defect energy levels are further confirmed by spin resolved atom projected density of states (PDOS) (Supplementary Figure S1). PDOS suggests that the contribution to the valance band in the vicinity of Fermi level is mainly due to Mo-d states in pristine MoS_2. In case of MoS_2 containing atomic defects, contribution to valance band arises from *S-p* orbitals while conduction band is due to both *Mo-d* and *S-p* orbitals for both the spins. For V_{MoS_2} type of defects Mo-d states contributes to the VBM while S-p (down spin) states contributes to CBM.

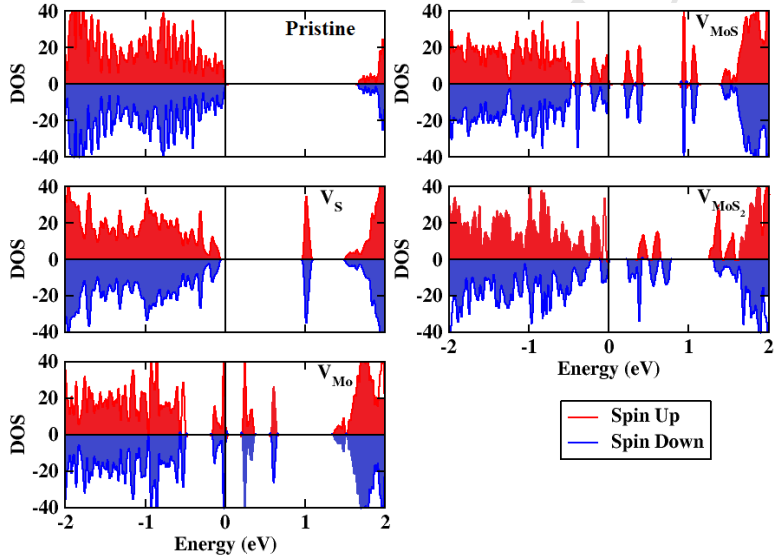

Figure 5. Spin polarized total density of states for atomic vacancies in monolayer MoS_2.

Next, we turn to determine the magnetic properties of MoS_2 with defects. We find that the atomic defects in MoS_2 do not lead to the magnetization in the system. Our result for the V_S is in agreement with the conclusions drawn by Jinhua Hong *et. al*. [53]. We find an induced magnetic moment of 1.88 μ_B for V_{MoS_2}. This induced magnetic moment for V_{MoS_2} can be attributed to asymmetry of spin up and spin down density of states (figure 5). Note that for rest of the vacancy types spin up and spin down density of states show symmetry, suggesting that electrons might have occupied same number of spin up and spin down states resulting into no net magnetization.

Also, spin density difference plot for the case of V_{MoS_2} (figure S2) suggest that maximum contribution to magnetic moment comes from Mo atoms which is consistent with the PDOS. Also, only nearest neighbor to vacancy site has asymmetric spin densities which confirms the presence of magnetic moment in the system.

3.2 Transport Properties

In monolayer with defects, the presence of defect energy levels in the vicinity of Fermi level is expected to modify electron transport properties as compared to the pristine monolayer. The expected modulation in conductance can be quantified by calculating the current-voltage characteristics using a model setup to mimic the scanning tunneling microscope (STM) measurements [54]. In this model set up a ferromagnetic cage like Fe_{13} cluster has been used to simulate the spin polarized probe tip of STM-like setup. The Bardeen, Tersoff and Hamann (BTH) formalism [55, 56] has been used to simulate tunneling characteristics for the considered system. The biasing is defined to be forward bias (or positive bias) when the sample is connected to the positive potential with electrons flowing from tip to sample. The tip sample distance is kept at 4Å to ensure the nonbonding configuration between tip and sample. It is worth mentioning here that the magnitude of current depends exponentially upon the tip-sample separation, although the tunneling characteristics remain the same.

The calculated spin resolved tunneling characteristics of the pristine and defective monolayers have been plotted in figure 6 between bias range of -0.5 V to +0.5 V. As the tunneling current is directly proportional to the convolution of DOS between the tip and sample, the finite spin-up and spin-down DOS in the vicinity of the Fermi level of defective monolayer is in principle the reason of increase in tunneling of both spin carriers (spin-up and spin-down) with the bias voltage. We find that the magnitude of current increases at low bias (at ±0.1 V) for both spin carriers which can be attributed to the presence of defect energy levels in defective monolayers. Interestingly, for V_{MoS_2} case magnitude of current due to spin up carriers modulates at higher bias as compared to spin down case. This could be attributed to difference in available spin up and

spin down channels in the vicinity of Fermi level (figure 3). This interesting feature underlines the potential of MoS_2 with V_{MoS_2} type defects in spin based electronic devices.

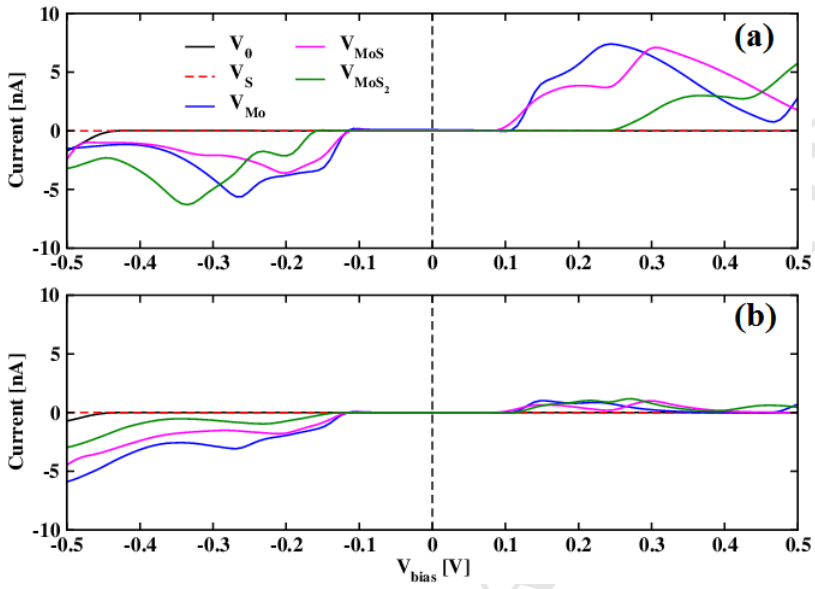

Figure 6: Spin polarized I-V Characteristics of pristine and defective MoS_2 monolayer; a) spin up, b) spin down.

3.3 Thermoelectric Properties

Our analysis suggests that MoS_2 monolayer with defects exhibits drastic change in electronic structures around Fermi level from that of pristine form. MoS_2 monolayer with atomic defects has strongly reduced band gap and an enhanced density of states around the Fermi level. Let us now examine how the thermoelectric properties of defective MoS_2 monolayer differ from that of pristine counterpart which has not been reported yet. The new energy levels in defective MoS_2 play a crucial role in determining the thermoelectric performance of material. A good thermoelectric material must be able to convert dissipating heat into electrical energy efficiently. The modulation in electronic properties of pristine MoS_2 with atomic defects is pointing to an expected influence on thermoelectric performance of MoS_2. Figure S3 – S5 (supplementary information) summarizes the calculated S, σ, σ S^2 as a function of chemical potential (μ) at different temperatures. In these calculations chemical potential is positive when Fermi level is raised (lowered), which corresponds to n-type (p-type) doping. The Seebeck coefficients are lower for V_{Mo} and V_{MoS} relative to pristine MoS_2. The maximum room temperature Seebeck

coefficient is ~1000 and (~500) μV/K for V_S and V_{MoS_2} respectively (Figure S3). The large Seebeck coefficients V_S and V_{MoS_2} is related to the fact that MoS_2 with such defects introduces new energy levels around the Fermi level leading to asymmetric density of states between valance band and conduction band resulting in high Seebeck coefficient. The Seebeck coefficient decreases with the increase in temperature, however, the values of S are comparable to earlier reported values at 300K [37].

The efficiency of thermoelectric materials could be enhanced by increasing Power Factor (σS^2). Despite the fact that the Seebeck coefficients for V_S and V_{MoS_2} are higher than the pristine MoS_2 and other cases, the conductivity (σ) has also a strong effect in controlling the Power Factor than the Seebeck coefficient. An enhancement in σ is observed for p-type doping for pristine and V_S case while for all other cases 'σ' continuously modulates with chemical potential (Figure S3 and S4). Note that relative to pristine MoS_2, MoS_2 with defects shows decreased conductivity (σ).

The figure of merit (ZT) is a key parameter to quantify the efficiency of thermoelectric materials and devices. The optimization of ZT value also depends on the electronic thermal conductivity (k_e) and phonon thermal conductivity (k_{ph}). The theoretical [30, 57] and experimental [31, 58] literature reports phonon thermal conductivity of monolayer and few-layer MoS_2 with values ranging from 0.24 $Wm^{-1}K^{-1}$ to 116.8 $Wm^{-1}K^{-1}$. Here we employed the experimental value of k_{ph}= 35.4 $Wm^{-1}K^{-1}$ by R. Yan *et. al.* [31] along with our calculated electronic thermal conductivity to calculate total thermal conductivity ($k = k_{ph} + k_e$). Figure S6 depicts calculated total thermal conductivity as a function of chemical potential at different temperatures for pristine and defective monolayer MoS_2. A significant reduction (10 times) in thermal conductivity has been found for the MoS_2 with defects. Relative to different types of considered atomic defects, V_S and V_{MoS_2} show highly reduced total thermal conductivity pointing towards an enhanced ZT.

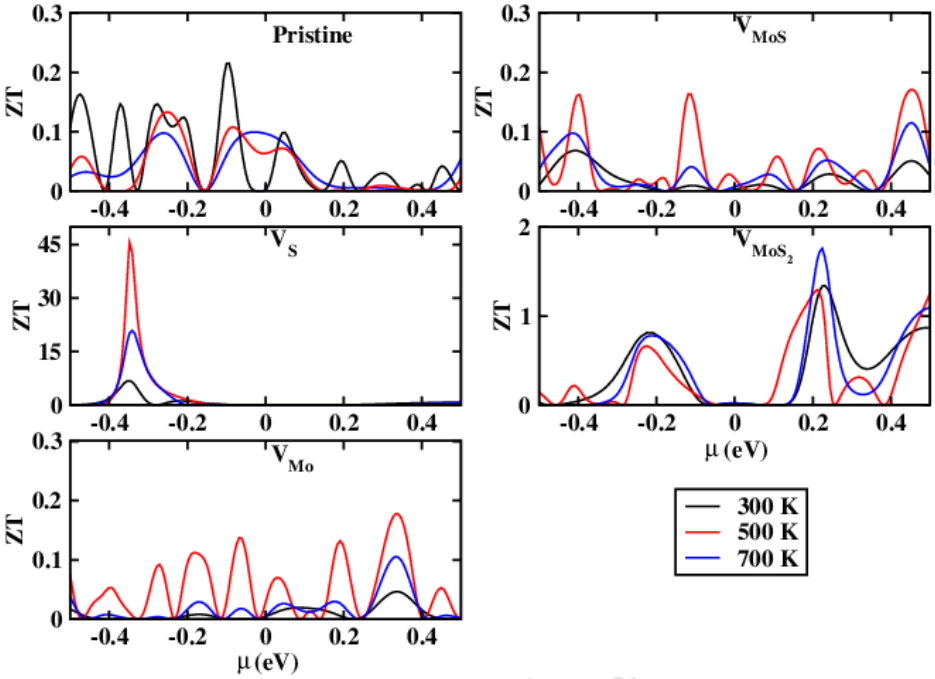

Figure 7: Calculated Figure of merit (ZT) for different atomic defects as a function of chemical potential at 300 K, 500 K and 700 K.

Figure 7 summarizes the figure of merit dependence on the chemical potential (μ) at 300, 500 and 700 K. The highest value of ZT is found to be 0.21 at 300 K which is in agreement with the earlier reported values ranging between 0.02 to 0.53 [37] for pristine MoS_2. The value of ZT modulates around 0.2 for the MoS_2 with defects. A room temperature (at 300 K) ZT of 6.24 and 1.30 has been calculated for V_S and V_{MoS_2}. An enhanced ZT for V_S (V_{MoS_2}) is attributed to higher (lower) Seebeck coefficient (electronic thermal conductivity). The thermoelectric properties also show tuneability with the temperature. Our results suggest that the atomic defects and temperature show enhancing influence on the thermoelectric properties of MoS_2 monolayer. It is worth mentioning here that SOC has great impact on electronic properties for the other TMD's as compared to MoS_2 which can essentially influence the power factor [18]. Therefore, these interesting results further allows to investigate the effect of SOC and temperature on the defective monolayer systems of other TMD's (MX_2; M=Mo, W; X=S, Se) which can possibly impact the modulation in figure of merit.

Conclusions

A first principle study has been carried out to study the electronic and thermoelectric properties of MoS_2 monolayer with atomic defects. Following can be concluded from this study:

- The defect formation energy for Sulphur defect is found to be +5.81 eV which is much lower than that found for other atomic defect cases.
- The reduction of interatomic distance by 2.66 % and 11.45 % around the defect sites is significant for V_{Mo} and V_{MoS_2} type defects, while for V_S and V_{MoS} type of vacancy atomic distortions are of the order of 0.05 Å.
- The electronic band gap shows tuneability with the atomic defects. Band gap gets reduced to 0.22 eV with a direct to indirect band gap transition due to appearance of defect energy levels.
- An induced magnetic moment of 1.88 μ_B has been found for V_{MoS_2} only.
- The magnitude of current increases at low bias (at ±0.1 V) for both spin carriers suggesting presence of defect energy levels in monolayers with defects.
- The thermoelectric properties including Seebeck coefficient, electrical and thermal conductivity, power factor and figure of merit show tuneability with temperature. The room temperature ZT of MoS_2 with S and MoS_2-type defects can reach as high as 6.24 and 1.30 respectively.

Thus, our investigations have systematically provided a significant understanding of the variation in electronic, magnetic, transport and thermoelectric properties induced by atomic defects which can be used as a reference point for exploring potential applications at nanoscale.

Acknowledgements

Munish Sharma wishes to acknowledge the DST, Govt. of India, New Delhi for providing the financial support in the form of INSPIRE Fellowship. CVRAMAN, high performance computing cluster (provided by FIST, DST, Govt. of India, New Delhi) at Physics Department, Himachal Pradesh University and K2 high performance computing cluster at IUAC have been used to obtain results presented in this paper.

References

[1] K.S. Novoselov, A.K. Geim, S.V. Morozov, D. Jiang, Y. Zhang, S.V. Dubonos, I.V. Grigorieva, A.A. Firsov, Electric field effect in atomically thin carbon films, science, 306 (2004) 666-669.

[2] A.C. Ferrari, F. Bonaccorso, V. Fal'Ko, K.S. Novoselov, S. Roche, P. Bøggild, S. Borini, F.H. Koppens, V. Palermo, N. Pugno, Science and technology roadmap for graphene, related two-dimensional crystals, and hybrid systems, Nanoscale, 7 (2015) 4598-4810.

[3] Z. Sun, H. Chang, Graphene and graphene-like two-dimensional materials in photodetection: mechanisms and methodology, Acs Nano, 8 (2014) 4133-4156.

[4] M. Sharma, A. Kumar, J.D. Sharma, P. Ahluwalia, Electronic and Dielectric Properties of Graphene Monoxide: A First Principle Study, Quantum Matter, 5 (2016) 315-318.

[5] J.D. Sharma, M. Sharma, N. Kumar, P. Ahluwalia, Computational study of dielectric function and optical properties of a graphane nano structure containing graphene quantum dot, in: Journal of Physics: Conference Series, IOP Publishing, 2013, pp. 012010.

[6] P. Miró, M. Audiffred, T. Heine, An atlas of two-dimensional materials, Chemical Society Reviews, 43 (2014) 6537-6554.

[7] E. Gourmelon, O. Lignier, H. Hadouda, G. Couturier, J. Bernede, J. Tedd, J. Pouzet, J. Salardenne, MS_2 (M= W, Mo) photosensitive thin films for solar cells, Solar energy materials and solar cells, 46 (1997) 115-121.

[8] H. Li, Z. Yin, Q. He, H. Li, X. Huang, G. Lu, D.W.H. Fam, A.I.Y. Tok, Q. Zhang, H. Zhang, Fabrication of single-and multilayer MoS_2 film-based field-effect transistors for sensing NO at room temperature, small, 8 (2012) 63-67.

[9] F.K. Perkins, A.L. Friedman, E. Cobas, P. Campbell, G. Jernigan, B.T. Jonker, Chemical vapor sensing with monolayer MoS_2, Nano letters, 13 (2013) 668-673.

[10] M. Sharma, P. Jamdagni, A. Kumar, P. Ahluwalia, R. Chitra, S. Bhattacharya, N. Sahoo, Interactions of gas molecules with monolayer $MoSe_2$: A first principle study, in: AIP Conference Proceedings, AIP Publishing, 2016, pp. 140045.

[11] M. Sharma, A. Kumar, P. Ahluwalia, Optical fingerprints and electron transport properties of DNA bases adsorbed on monolayer MoS_2, RSC Advances, 6 (2016) 60223-60230.

[12] Z. Liu, J. Yang, F. Grey, J.Z. Liu, Y. Liu, Y. Wang, Y. Yang, Y. Cheng, Q. Zheng, Observation of microscale superlubricity in graphite, Physical review letters, 108 (2012) 205503.

[13] M. Buscema, M. Barkelid, V. Zwiller, H.S. van der Zant, G.A. Steele, A. Castellanos-Gomez, Large and tunable photothermoelectric effect in single-layer MoS_2, Nano letters, 13 (2013) 358-363.

[14] K.-K. Liu, W. Zhang, Y.-H. Lee, Y.-C. Lin, M.-T. Chang, C.-Y. Su, C.-S. Chang, H. Li, Y. Shi, H. Zhang, Growth of large-area and highly crystalline MoS_2 thin layers on insulating substrates, Nano letters, 12 (2012) 1538-1544.

[15] K.F. Mak, C. Lee, J. Hone, J. Shan, T.F. Heinz, Atomically thin MoS_2: a new direct-gap semiconductor, Physical Review Letters, 105 (2010) 136805.

[16] Y. Yoon, K. Ganapathi, S. Salahuddin, How good can monolayer MoS_2 transistors be?, Nano letters, 11 (2011) 3768-3773.

[17] D. Xiao, G.-B. Liu, W. Feng, X. Xu, W. Yao, Coupled spin and valley physics in monolayers of MoS_2 and other group-VI dichalcogenides, Physical Review Letters, 108 (2012) 196802.

[18] S.-D. Guo, J.-L. Wang, Spin–orbital coupling effect on the power factor in semiconducting transition-metal dichalcogenide monolayers, Semiconductor Science and Technology, 31 (2016) 095011.

[19] Y. Cheng, Z. Zhu, M. Tahir, U. Schwingenschlögl, Spin-orbit–induced spin splittings in polar transition metal dichalcogenide monolayers, EPL (Europhysics Letters), 102 (2013) 57001.
[20] B. Radisavljevic, A. Radenovic, J. Brivio, i.V. Giacometti, A. Kis, Single-layer MoS_2 transistors, Nature nanotechnology, 6 (2011) 147-150.
[21] J.N. Coleman, M. Lotya, A. O'Neill, S.D. Bergin, P.J. King, U. Khan, K. Young, A. Gaucher, S. De, R.J. Smith, Two-dimensional nanosheets produced by liquid exfoliation of layered materials, Science, 331 (2011) 568-571.
[22] H. Schmidt, S. Wang, L. Chu, M. Toh, R. Kumar, W. Zhao, A. Castro Neto, J. Martin, S. Adam, B. Özyilmaz, Transport properties of monolayer MoS_2 grown by chemical vapor deposition, Nano letters, 14 (2014) 1909-1913.
[23] Y.H. Lee, X.Q. Zhang, W. Zhang, M.T. Chang, C.T. Lin, K.D. Chang, Y.C. Yu, J.T.W. Wang, C.S. Chang, L.J. Li, Synthesis of Large-Area MoS_2 Atomic Layers with Chemical Vapor Deposition, Advanced Materials, 24 (2012) 2320-2325.
[24] Q. Feng, Y. Zhu, J. Hong, M. Zhang, W. Duan, N. Mao, J. Wu, H. Xu, F. Dong, F. Lin, Growth of Large-Area 2D $MoS_{2(1-x)}$ Se_{2x} Semiconductor Alloys, Advanced Materials, 26 (2014) 2648-2653.
[25] H.-P. Komsa, J. Kotakoski, S. Kurasch, O. Lehtinen, U. Kaiser, A.V. Krasheninnikov, Two-dimensional transition metal dichalcogenides under electron irradiation: defect production and doping, Physical review letters, 109 (2012) 035503.
[26] Z. Yu, Y. Pan, Y. Shen, Z. Wang, Z.-Y. Ong, T. Xu, R. Xin, L. Pan, B. Wang, L. Sun, Towards intrinsic charge transport in monolayer molybdenum disulfide by defect and interface engineering, Nature communications, 5 (2014).
[27] S. Najmaei, Z. Liu, W. Zhou, X. Zou, G. Shi, S. Lei, B.I. Yakobson, J.-C. Idrobo, P.M. Ajayan, J. Lou, Vapour phase growth and grain boundary structure of molybdenum disulphide atomic layers, Nature materials, 12 (2013) 754-759.
[28] J. Xie, H. Zhang, S. Li, R. Wang, X. Sun, M. Zhou, J. Zhou, X.W.D. Lou, Y. Xie, Defect-rich MoS_2 ultrathin nanosheets with additional active edge sites for enhanced electrocatalytic hydrogen evolution, Advanced Materials, 25 (2013) 5807.
[29] X. Liu, G. Zhang, Q.-X. Pei, Y.-W. Zhang, Phonon thermal conductivity of monolayer MoS_2 sheet and nanoribbons, Applied Physics Letters, 103 (2013) 133113.
[30] Y. Cai, J. Lan, G. Zhang, Y.-W. Zhang, Lattice vibrational modes and phonon thermal conductivity of monolayer MoS_2, Physical Review B, 89 (2014) 035438.
[31] R. Yan, J.R. Simpson, S. Bertolazzi, J. Brivio, M. Watson, X. Wu, A. Kis, T. Luo, A.R. Hight Walker, H.G. Xing, Thermal conductivity of monolayer molybdenum disulfide obtained from temperature-dependent Raman spectroscopy, ACS nano, 8 (2014) 986-993.
[32] J. Wu, H. Schmidt, K.K. Amara, X. Xu, G. Eda, B. Özyilmaz, Large thermoelectricity via variable range hopping in chemical vapor deposition grown single-layer MoS_2, Nano letters, 14 (2014) 2730-2734.
[33] K. Hippalgaonkar, Y. Wang, Y. Ye, D.Y. Qiu, H. Zhu, Y. Wang, J. Moore, S.G. Louie, X. Zhang, High thermoelectric power factor in two-dimensional crystals of MoS_2, Physical Review B, 95 (2017) 115407.
[34] S. Konabe, T. Yamamoto, Valley photothermoelectric effects in transition-metal dichalcogenides, Physical Review B, 90 (2014) 075430.
[35] M. Tahir, U. Schwingenschlögl, Tunable thermoelectricity in monolayers of MoS_2 and other group-VI dichalcogenides, New Journal of Physics, 16 (2014) 115003.
[36] Y. Zhao, Z. Dai, C. Zhang, C. Lian, S. Zeng, G. Li, S. Meng, J. Ni, Intrinsic electronic transport and thermoelectric power factor in n-type doped monolayer MoS_2, New Journal of Physics, 20 (2018) 043009.

[37] Z. Jin, Q. Liao, H. Fang, Z. Liu, W. Liu, Z. Ding, T. Luo, N. Yang, A revisit to high thermoelectric performance of single-layer MoS_2, Scientific reports, 5 (2015).
[38] H. Karamitaheri, M. Pourfath, R. Faez, H. Kosina, Geometrical effects on the thermoelectric properties of ballistic graphene antidot lattices, Journal of Applied Physics, 110 (2011) 054506.
[39] Z. Ding, Q.-X. Pei, J.-W. Jiang, Y.-W. Zhang, Manipulating the thermal conductivity of monolayer MoS_2 via lattice defect and strain engineering, The Journal of Physical Chemistry C, 119 (2015) 16358-16365.
[40] J.-Y. Kim, S.-M. Choi, W.-S. Seo, W.-S. Cho, Thermal and electronic properties of exfoliated metal chalcogenides, Bulletin of the Korean Chemical Society, 31 (2010) 3225-3227.
[41] Y. Ouyang, J. Guo, A theoretical study on thermoelectric properties of graphene nanoribbons, Applied Physics Letters, 94 (2009) 263107.
[42] H. Zhang, G. Lee, K. Cho, Thermal transport in graphene and effects of vacancy defects, Physical Review B, 84 (2011) 115460.
[43] S. Chen, Q. Wu, C. Mishra, J. Kang, H. Zhang, K. Cho, W. Cai, A.A. Balandin, R.S. Ruoff, Thermal conductivity of isotopically modified graphene, Nature materials, 11 (2012) 203-207.
[44] G. Kresse, J. Furthmüller, Efficiency of ab-initio total energy calculations for metals and semiconductors using a plane-wave basis set, Computational Materials Science, 6 (1996) 15-50.
[45] G. Kresse, D. Joubert, From ultrasoft pseudopotentials to the projector augmented-wave method, Physical Review B, 59 (1999) 1758-1775.
[46] P.E. Blöchl, Projector augmented-wave method, Physical Review B, 50 (1994) 17953.
[47] J.P. Perdew, P. Ziesche, H. Eschrig, Electronic structure of solids' 91, Akademie Verlag, Berlin, 1991.
[48] G.K. Madsen, D.J. Singh, BoltzTraP. A code for calculating band-structure dependent quantities, Computer Physics Communications, 175 (2006) 67-71.
[49] Q. Yue, S. Chang, S. Qin, J. Li, Functionalization of monolayer MoS_2 by substitutional doping: a first-principles study, Physics Letters A, 377 (2013) 1362-1367.
[50] Y. Cheng, Z. Zhu, W. Mi, Z. Guo, U. Schwingenschlögl, Prediction of two-dimensional diluted magnetic semiconductors: doped monolayer MoS_2 systems, Physical Review B, 87 (2013) 100401.
[51] A. Splendiani, L. Sun, Y. Zhang, T. Li, J. Kim, C.-Y. Chim, G. Galli, F. Wang, Emerging photoluminescence in monolayer MoS_2, Nano letters, 10 (2010) 1271-1275.
[52] S. Lebegue, O. Eriksson, Electronic structure of two-dimensional crystals from ab initio theory, Physical Review B, 79 (2009) 115409.
[53] J. Hong, Z. Hu, M. Probert, K. Li, D. Lv, X. Yang, L. Gu, N. Mao, Q. Feng, L. Xie, Exploring atomic defects in molybdenum disulphide monolayers, Nature communications, 6 (2015).
[54] D. Tománek, S.G. Louie, First-principles calculation of highly asymmetric structure in scanning-tunneling-microscopy images of graphite, Physical Review B, 37 (1988) 8327.
[55] J. Tersoff, D. Hamann, Theory and application for the scanning tunneling microscope, Physical review letters, 50 (1983) 1998.
[56] R.M. Feenstra, J.A. Stroscio, A. Fein, Tunneling spectroscopy of the Si (111) 2×1 surface, Surface science, 181 (1987) 295-306.
[57] W. Li, J. Carrete, N. Mingo, Thermal conductivity and phonon linewidths of monolayer MoS_2 from first principles, Applied Physics Letters, 103 (2013) 253103.
[58] C. Muratore, V. Varshney, J.J. Gengler, J. Hu, J.E. Bultman, T.M. Smith, P.J. Shamberger, B. Qiu, X. Ruan, A.K. Roy, Cross-plane thermal properties of transition metal dichalcogenides, Applied Physics Letters, 102 (2013) 081604.

Highlights

- We find tuneability of band gap and thermoelectric figure of merit with the atomic defects.
- The spin-polarized character of the monolayer with defects is clearly captured by the tunneling current calculated in the STM-like setup.
- A relatively low thermal conductivity has been observed in monolayers with defects as compared to pristine form resulting in enhanced room temperature figure of merit as high as 6.24 and 1.30 respectively.